

## Deterministic assembly of 3D mesostructures in advanced materials via compressive buckling: A short review of recent progress



Zheng Yan<sup>a,1</sup>, Mengdi Han<sup>b,1</sup>, Yiyuan Yang<sup>a</sup>, Kewang Nan<sup>a</sup>, Haiwen Luan<sup>c</sup>, Yiyue Luo<sup>a</sup>, Yihui Zhang<sup>d</sup>, Yonggang Huang<sup>c</sup>, John A. Rogers<sup>a,e,f,g,\*</sup>

<sup>a</sup> Department of Materials Science and Engineering and Frederick Seitz Materials Research Laboratory, University of Illinois at Urbana-Champaign, Urbana, IL 61801, USA

<sup>b</sup> National Key Laboratory of Science and Technology on Micro/Nano Fabrication, Peking University, Beijing 100871, PR China

<sup>c</sup> Departments of Civil and Environmental Engineering, Mechanical Engineering and Materials Science and Engineering, Center for Engineering and Health, and Skin Disease Research Center, Northwestern University, Evanston, IL 60208, USA

<sup>d</sup> Center for Mechanics and Materials, AML, Department of Engineering Mechanics, Tsinghua University, Beijing 100084, PR China

<sup>e</sup> Departments of Materials Science and Engineering, Biomedical Engineering, Chemistry, Mechanical Engineering, Electrical Engineering and Computer Science, and Neurological Surgery, Northwestern University, Evanston, IL 60208, USA

<sup>f</sup> Center for Bio-Integrated Electronics, Northwestern University, Evanston, IL 60208, USA

<sup>g</sup> Simpson Querrey Institute for Nano/biotechnology, Northwestern University, Evanston, IL 60208, USA

### ARTICLE INFO

#### Article history:

Received 15 October 2016

Received in revised form

19 December 2016

Accepted 25 December 2016

Available online 27 December 2016

#### Keywords:

Deterministic assembly

Compressive buckling

3D mesostructures

Advanced materials

### ABSTRACT

Nearly all micro/nanosystems found in biology have function that is intrinsically enabled by hierarchical, three-dimensional (3D) designs. Compelling opportunities exist in exploiting similar 3D architectures in man-made devices for applications in biomedicine, sensing, energy storage and conversion, electronics and many other areas of advanced technology. Although a lack of practical routes to the required 3D layouts has hindered progress to date, recent advances in mechanically-guided 3D assembly have the potential to provide the required access to wide-ranging structural geometries, across a broad span of length scales, in a way that leverages the most sophisticated materials and design concepts that exist in state-of-the-art 2D microsystems. This review summarizes the key concepts and illustrates their use in four major categories of 3D mesostructures: open filamentary frameworks, mixed structures of membranes/filaments (Kirigami-inspired structures), folded constructs (Origami-inspired structures) and overlapping, nested and entangled networks. The content includes not only previously published examples, but also several additional illustrative cases. A collection of 3D starfish-like and jellyfish-like structures with critical dimensions that span nearly a factor of ten million, from one hundred nanometers to nearly one meter, demonstrates the scalability of the process.

© 2017 Elsevier Ltd. All rights reserved.

### Contents

1. Introduction.....	97
2. Discussion.....	97
2.1. Assembly of 3D filamentary mesostructures.....	97
2.2. Assembly of 3D mixed mesostructures of membranes and filaments.....	98
2.3. Assembly of 3D folded mesostructures.....	100
2.4. Assembly of 3D overlapping, nested and entangled networks.....	101

\* Corresponding author at: Department of Materials Science and Engineering and Frederick Seitz Materials Research Laboratory, University of Illinois at Urbana-Champaign, Urbana, IL 61801, USA.

E-mail address: [jrogers@illinois.edu](mailto:jrogers@illinois.edu) (J.A. Rogers).

<sup>1</sup> These authors contributed equally to this work.

2.5. Assembly of 3D structures in variety of materials spanning wide length scales .....	103
3. Conclusion and outlook .....	103
Acknowledgments .....	103
References.....	103

## 1. Introduction

Three-dimensional mesostructures with controllable shapes and dimensions can be exploited in various classes of micro/nanotechnologies such as micro/nano-electro-mechanical systems (MEMS/NEMS) [1–3], biomedical devices [4–6], electronics and optoelectronics [7–9], batteries and supercapacitors [10–12], metamaterials [13–15], robotics [16–18] and others. Diverse manufacturing techniques, such as 3D printing and two-photon/multiphoton lithography [19–22], self-assembly [23,24] and templated growth [25,26], can form 3D structures with certain types of shapes at different scales. These approaches, however, are (i) applicable only to limited classes of materials, generally excluding, as examples, device-grade inorganic semiconductors such as silicon and GaAs; (ii) incompatible with the exceptionally advanced lithographic techniques that are routinely used in manufacturing of conventional 2D devices. These limitations restrict the range of structural and functional options, the device performance, and the production efficiency of micro/nanosystems with 3D layouts. Approaches that utilize strain-induced bending/folding [27,28] avoid some of these drawbacks and offer many attractive features, but they operate most effectively with only certain classes of 3D geometries.

Recent research establishes concepts for realizing 3D mesostructures in advanced materials and device architectures by assembly processes driven by compressive buckling [29–32]. This scheme exploits thin, 2D precursors fabricated using the most sophisticated materials processes available in state-of-the-art planar technologies. Lithographically defining a set of chemically activated sites followed by transfer printing [33,34] onto a prestrained elastomer substrate leads to strong covalent bonding at these locations. Releasing the prestrain creates compressive forces that induce out-of-plane geometric extension, including complex combinations of translational and rotational motions, of the non-bonded regions of the 2D structures. The result yields 3D architectures with programmed configurations in a continuous and reversible manner. This 3D assembly approach is naturally compatible with existing planar microsystems technologies and it provides a fast, powerful means for building complex, 3D structures and device layouts in a parallel fashion, over a wide length scales. Published demonstration examples include over 200 different 3D mesostructures, where materials include inorganic semiconductors, polymers, metals and their heterogeneous combinations, and length scales span from nanometers to meters. An additional feature of the resulting 3D structures is that they are naturally tethered to elastomers, thereby providing means for reversible mechanical tuning of the geometries, and for achieving advanced electrical, optical and magnetic function in systems that have low effective moduli and high levels of stretchability.

This review article discusses the design concepts and assembly techniques organized around four major categories of 3D mesostructures: (1) open filamentary frameworks (Section 2.1), (2) mixed structures of membranes/filaments (Kirigami-inspired structures; Section 2.2), (3) folded constructs (Origami-inspired structures; Section 2.3) and (4) overlapping, nested and entangled networks (Section 2.4). In each case, key considerations include the overall shapes, patterns of cuts, thickness distributions, and multi-layer configurations associated with the 2D precursors, the magnitude and orientation of prestrain in the elastomeric assembly

substrate, and the numbers and locations of bonding sites. The associated processing techniques include advanced methods in micro/nano fabrication, etching, transfer printing, surface chemistry patterning, controlled buckling, sacrificial layer incorporation, mechanical/laser cutting and micromanipulation. In addition to previously reported structures, several new examples presented here illustrate important points. Section 2.5 highlights the dimensional scalability of the process, through demonstrations of 3D starfish-like and jellyfish-like structures with critical dimensions that span seven orders of magnitude.

## 2. Discussion

### 2.1. Assembly of 3D filamentary mesostructures

The first category of 3D mesostructures consists of networks of filamentary ribbons [29]. Fig. 1(a) highlights the general assembly procedures using a simple 3D helical structure as an example. The process starts with the micro/nano fabrication of a 2D serpentine precursor on a planar temporary substrate via well-established techniques in photolithography and thin film etching. The next step involves retrieval of the precursor onto a water soluble tape by elimination of an underlying sacrificial layer, in a way that exposes the backside surface. Lithographic patterning and surface chemical treatments, typically involving the formation of  $-OH$  groups, defines bonding sites with sub-micron spatial precision. Transfer onto a prestrained silicone elastomer (prestrain level defined as  $\varepsilon_{pre} = \Delta L/L$ , where  $L$  is the original length and  $\Delta L$  is the increment compared with  $L$ ), also chemically functionalized with  $-OH$  surface groups, leads to strong adhesion at the bonding sites due to covalent bonds that result from interfacial condensation reactions. These covalent linkages lead to interfaces with work of adhesion  $>8\text{ J/m}^2$ , well above weak van der Waals forces-dominated interfacial interactions at non-bonded locations, where the work of adhesion is  $\sim 0.2\text{ J/m}^2$  [29]. Releasing the prestrain returns the silicone to its original shape, thereby imparting large compressive forces onto the precursor at the points of strong bonding. Since the thicknesses ( $t$ ) of the ribbons are typically many times smaller than the widths ( $w$ ), the out-of-plane bending stiffness ( $\propto wt^3$ ) is much smaller than the in-plane value ( $\propto w^3t$ ). The effect is, therefore, to induce a complex, coordinated interplay of translational and rotational out-of-plane motions at the non-bonded regions, which in the case illustrated here leads to the formation of a 3D helix. The image in Fig. 1(b) shows a structure of this type made of single-crystal silicon (2  $\mu\text{m}$  in thickness, 50  $\mu\text{m}$  in width,  $\varepsilon_{pre} \approx 70\%$ ). With different 2D precursor geometries and bonding sites, this same overall process can be extended to classes of structures such as dual helices (Fig. 1(c)) and nested coaxial systems (Fig. 1(d)). In all cases, finite-element analysis (FEA) predictions (right frames in Fig. 1(b)–(d)) are highly consistent with the experimental results (left frames in Fig. 1(b)–(d)). Using FEA as a guide, the process design can be selected to limit maximum strains in the 3D structures to values that are well below the fracture thresholds of the constituent materials (e.g.  $\sim 1\%$  for single crystalline silicon).

Much more complex 3D structures can be assembled with different 2D precursors and distributions of bonding sites, and with other types of prestrain, including biaxial (Fig. 1(e)–(k)). The results in Fig. 1(h) demonstrate that for the same filamentary pentagram shape and the same  $\varepsilon_{pre}$  ( $\sim 50\%$ ) in a 2D precursor of

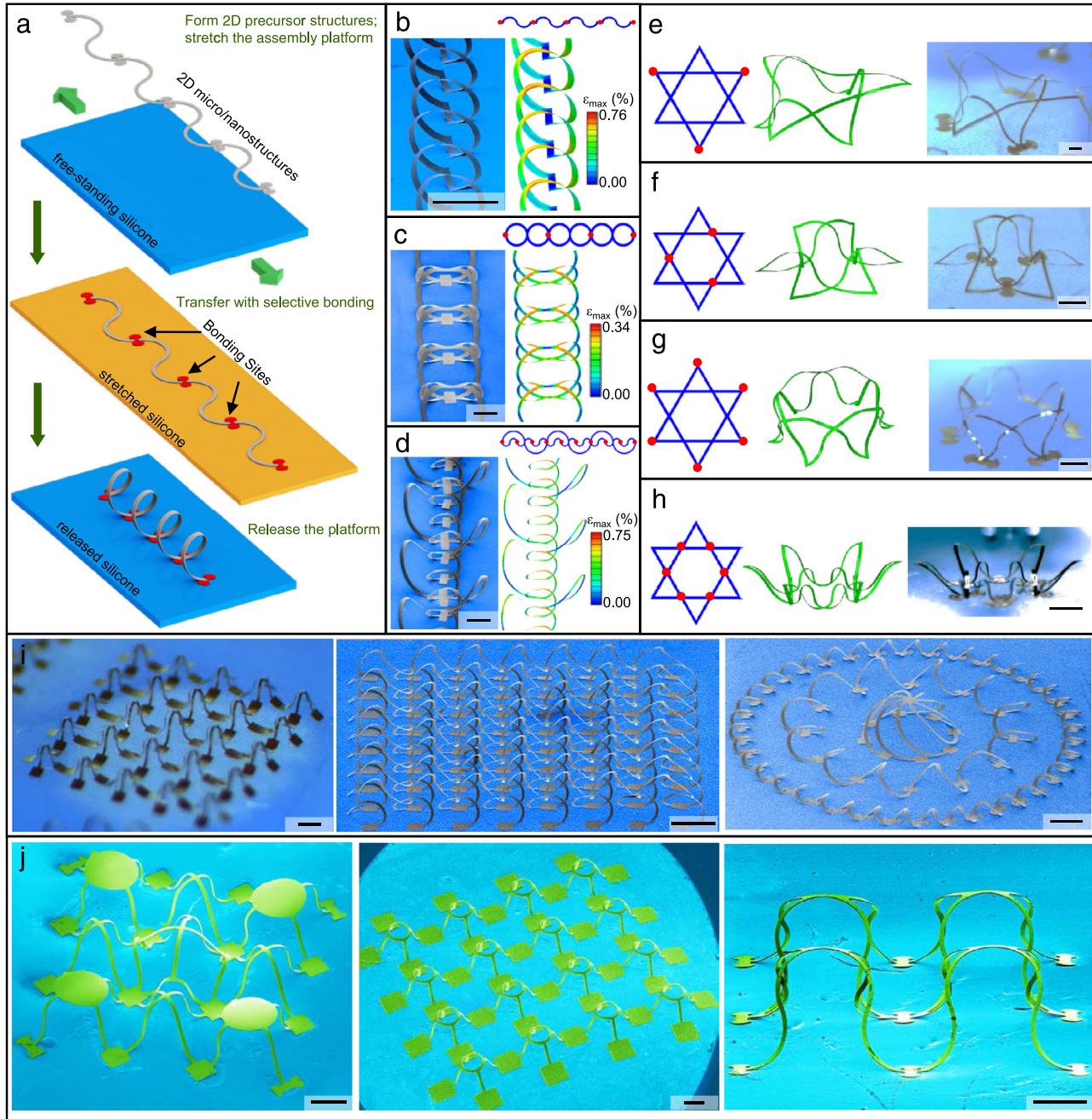


**Fig. 1.** 3D filamentary mesostructures. (a) Schematic illustration of the assembly process. From the top to the bottom: forming 2D micro/nanostructures using lithographic and etching techniques, transferring these structures to a stretched silicone elastomer with bonding at selected sites, releasing the elastomer to form 3D mesostructures. (b-d) Schematic diagram of 2D precursors with bonding sites marked in red (top), and corresponding SEM images (left) and FEA predictions (right). (e-h) Schematic diagram of 2D precursors with the same shapes but different configurations of bonding sites (left), and corresponding FEA predictions (middle) and SEM images (right). (i) 3D tent array, 8 × 8 double-floor networks and flower-like mesostructures made of silicon. (j) 3D table-tent mixed array, 4 × 4 raised ring array and 2 × 2 raised roof array made of bilayers of metal (Au) and polymer (polyimide). Scale bars, 400  $\mu\text{m}$ . (For interpretation of the references to color in this figure legend, the reader is referred to the web version of this article.)

Source: Reproduced from Xu et al. [29], with permission from American Association for the Advancement of Science.

silicon, different numbers and locations of bonding points lead to remarkably different 3D structures. As before, FEA analysis quantitatively captures all of these shapes, thereby indicating the utility of computation in rapidly exploring different design possibilities, with particular value for complex topographies. The left frame in Fig. 1(i) shows an example of 5 × 5 array of tent structures in filaments of silicon. Other examples include an 8 × 8 double-floor 3D helix structure (the middle frame in Fig. 1(i)) and a 3D flower-like construct with a concentric pair of toroids and a hemispherical cage in the center (the right frame in Fig. 1(i)). Three

filamentary 3D mesostructures made of bilayers of polyimide and gold, including a mixed array of tables and tents, a 4 × 4 raised ring array, and a 2 × 2 roof array, appear in Fig. 1(j) ( $\varepsilon_{\text{pre}} \approx 50\%$  for all cases here).

## 2.2. Assembly of 3D mixed mesostructures of membranes and filaments

Unlike collections of filamentary structures, membranes demonstrate considerable lateral constraints when subjected to bending.

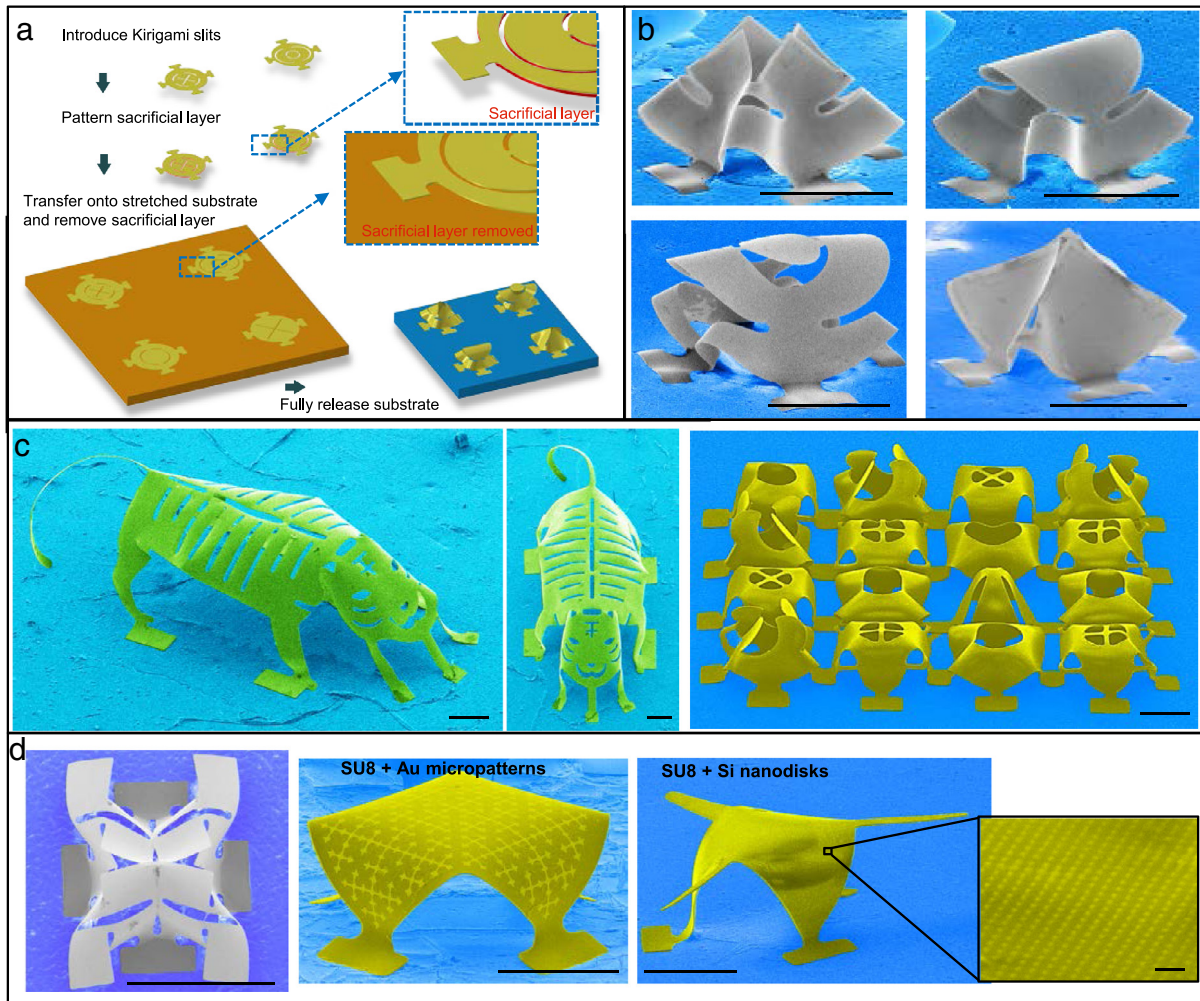


**Fig. 2.** 3D Kirigami mesostructures. (a) Schematic illustration of the fabrication process: forming 2D micro/nanomembrane with different patterns of cuts and underlying sacrificial layer, removing the sacrificial layer to create a gap, releasing prestrain to form 3D Kirigami structures. (b) SEM images of four 3D Kirigami structures with the same basic 2D precursor shape but different patterns of cuts; the examples here are made of bilayers of silicon nanomembranes and epoxy films. (c) Complex 3D Kirigami structures made of polymers, including an object made of polyimide ( $\sim 10 \mu\text{m}$  in thickness) that resembles a tiger (left), and a mixed array of hybrid membrane-ribbon structures (right) made of epoxy ( $\sim 4 \mu\text{m}$  in thickness). (d) 3D Kirigami structures with extended features, including a fractal-inspired pattern with two-order cross cuts (left), epoxy structures with Au micropatterns (middle) and silicon nanodisks (right). Scale bars, 200  $\mu\text{m}$ .

Source: Reproduced from Zhang et al. [30], with permission from National Academy of Sciences.

As a result, they undergo in-plane stretching in addition to out-of-plane bending in their final configuration after compressive buckling. Depending on the nature of boundary conditions (i.e., imposed constraints required for their buckling), the bend–stretch coupling has the potential to lead to localized stress concentrators of high strain energy that can lead to mechanical failure. Furthermore, the out-of-plane buckling process can be frustrated by forces of van der Waals-induced surface stiction to the assembly substrate at the non-bonding regions. These forces increase with the total contact area, and are typically much larger for membranes than for ribbons [29]. Strain relief concepts inspired by ideas adopted from the paper folding art of Kirigami can avoid these limitations. In particular, introduction of precisely engineered cuts and slits, enabled by photolithography and etching, at strategic locations across a 2D precursor can dramatically reduce local strain concentrations that arise during controlled compression [30]. Surface stiction can be minimized by including a sacrificial layer underneath non-bonding regions of the planar precursors, whose removal eliminates adhesion entirely by creating physical separation from the assembly substrate immediately before release of prestrain (Fig. 2(a)). These two methods allow formation of a wide range of structures that include both membranes and filaments, in elaborate 3D layouts, with

the same level of material diversity and size scalability as with the purely filamentary networks.

The Kirigami-inspired cuts and slits are essential in the context not only of strain-relief mechanics, as described above, but also design flexibility. Fig. 2(b) demonstrates a series of 3D structures made of bilayers of nanomembranes of device-grade silicon (300 nm in thickness) and photodefinition epoxy (SU8; 300 nm in thickness), where the differences arise only from the patterns of cuts, defined here by photolithography and reactive ion etching. Complex examples shown in Fig. 2(c) include a pop-up Kirigami ‘tiger’ formed with a non-equal biaxial prestrain ( $\varepsilon_{x,\text{pre}} \approx 100\%$ ,  $\varepsilon_{y,\text{pre}} \approx 33\%$ ) and an array of randomly mixed unit cells formed with equal biaxial prestrain ( $\varepsilon_{\text{pre}} \approx 60\%$ ), micro-fabricated using polyimide (10  $\mu\text{m}$  in thickness) and epoxy (4  $\mu\text{m}$  in thickness) respectively. Nanoscale structures of device-grade semiconductors and surface features can be easily integrated with the membranes. The left frame of Fig. 2(d) highlights a 3D structure with 1st and 2nd order cross cuts in a bilayer that consists of a silicon nanomembrane (300 nm in thickness) and a film of epoxy (300 nm in thickness). The center and right frames of Fig. 2(d) demonstrate hybrid structures of epoxy with gold micropatterns and silicon nanodisks, respectively. Capabilities in

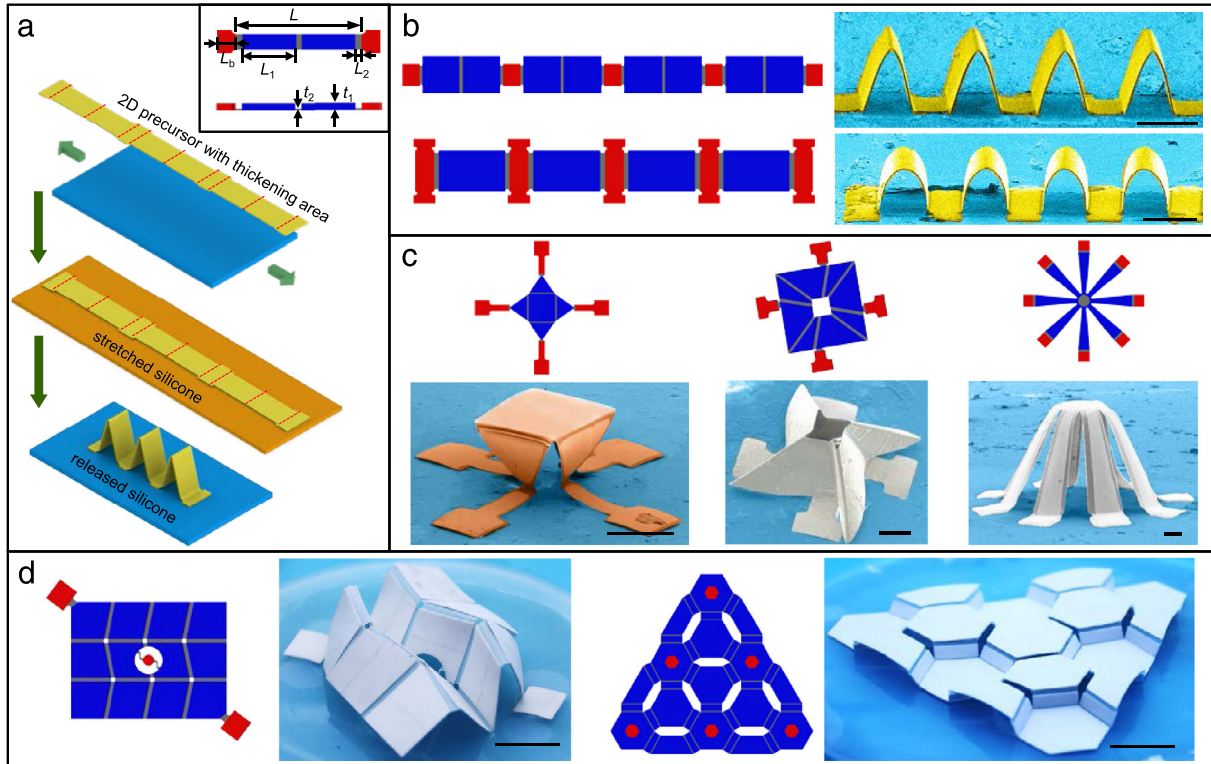


**Fig. 3.** 3D Origami mesostructures. (a) Schematic illustration of the fabrication process for 3D Origami mesostructures. From the top to the bottom: forming 2D precursors with non-uniform thicknesses design to yield folds at desired locations, transferring to a stretched silicone elastomer, releasing the elastomer to form 3D Origami structures. The inset illustrates the defined parameters in Eq. (1). (b) Schematic diagram of 2D precursors (left) and SEM images of 3D Origami structures of epoxy formed through uniaxial compression. (c) Schematic diagram of 2D precursors (top) and SEM images (bottom) of 3D Origami structures formed through biaxial compression. The structure in the left frame is made of gold and epoxy bilayers, and structures in the middle and right frames are made of silicon and epoxy bilayers. (d) 2D precursors (left) and optical images (right) of 3D Origami mesostructures made of plastic films with hierarchical forms of folding. The scale bars of SEM and optical images are 200  $\mu\text{m}$  and 20 mm, respectively. (For interpretation of the references to color in this figure legend, the reader is referred to the web version of this article.)  
Source: Reproduced from Yan et al. [31], with permission from Wiley.

integrating micro/nanopatterned, advanced electronic materials (metals, semiconductors) onto such platforms suggest routes to 3D microsystems such as transistors, sensors and actuators, with unique options in 3D design. The results could provide unusual electromagnetic or optoelectronic functions that would be difficult or impossible to access through conventional approaches.

### 2.3. Assembly of 3D folded mesostructures

The structures described in the previous two sections rely on global bending and twisting deformations, with smoothly varying levels of curvature defined by the 2D precursor geometry, the bonding sites and the prestrain in the assembly substrate. Many desired 3D structures demand spatial localization of the bending, to reproduce the type of folds that occur in Origami [31]. Control over the spatial distributions of thickness in the 2D precursors provides this sort of capability. Specifically, FEA simulations show that small thickness ratios ( $t_2/t_1 < 1/3$ ) and length ratios ( $L_2/L < 1/10$ ) between the regions targeted for creases ( $t_2$  and  $L_2$ ) and the other regions ( $t_1$  and  $L$ ) lead to Origami-like folding upon compressive buckling. Generally, the optimized parameters (such as  $t_2/t_1 < 1/3$ ) have broad applicability to different materials and prestrain levels, which can be used as a guidance in the design of various folded mesostructures. Based on the assumptions that the elastomer relaxes to 0% strain and the deformed configurations of creases are circular arcs, the geometry of the folding structures can be governed by:

$$\frac{3L_2}{L} \frac{1}{\theta_{fold}} \sin \frac{\theta_{fold}}{2} + \left( \frac{1}{2} - \frac{3L_2}{2L} \right) \cos \frac{\theta_{fold}}{2}$$

$$+ \frac{L_b}{2L} - \frac{1}{2(1 + \varepsilon_{pre})} \left( 1 + \frac{L_b}{L} \right) = 0 \quad (1)$$

where  $\theta_{fold}$  is the folding angle determined by prestrain ( $\varepsilon_{pre}$ ),  $L$  is the total length of the ribbon without bonding areas, and  $L_b$  is the length of the bonding region, respectively. Since the deformations of such structures are mainly accommodated by the creases, design considerations must include control of the maximum principal strain, and optimization of the ratios  $t_2/L_2$ ,  $t_2/t_1$ . Fig. 3(a) illustrates the defined parameters in Eq. (1) (inset) and demonstrates the procedures for making 3D folded mesostructures. Regions with potential to fold (red dotted lines) can be defined in the 2D precursor through lithographically patterned addition of layers in other areas. Release of the prestrain causes the non-bonded regions to buckle out of the plane and locally deform along targeted folds to guide the formation of 3D mesostructures with sharp variations in curvature.

A diverse range of Origami-inspired 3D geometries can be formed using these concepts through unidirectional, bidirectional, and even hierarchical folding as demonstrated in Fig. 3(b)–(d). Fig. 3(b) shows two representative examples formed through uniaxial compression with 2D precursors in the left panels and SEM images of 3D structures in the right panels. The top 3D structure consists of a periodic array of triangular columns made of polymer (epoxy) with folds (gray) located at the center and two ends. The corresponding example at the bottom exhibits periodic arc-shaped geometries with creases (gray) only at the two ends. For both cases, the thicknesses of the creases are 2  $\mu\text{m}$ , and the thicknesses of the other regions are 6  $\mu\text{m}$ . Fig. 3(c) demonstrates complex Origami mesostructures achieved by using equal biaxial pre-strain. The top

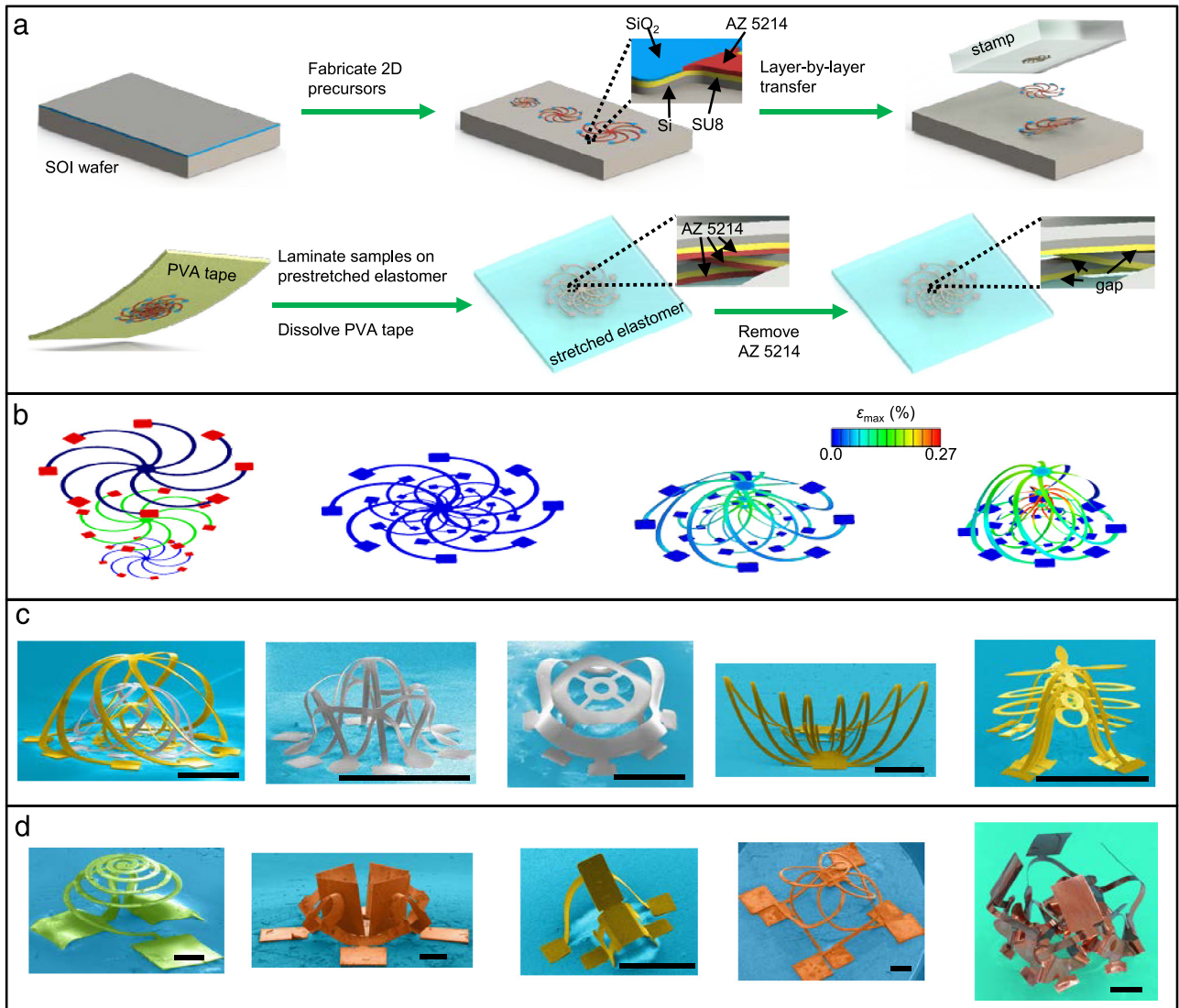


**Fig. 4.** 3D multilayer mesostructures. (a–b) Schematic illustration of the assembly process for 3D trilayer nested cages. (c) SEM images of 3D multilayer mesostructures with fully separated configurations. From left to right: trilayer nested cages of epoxy and silicon hybrids, bilayer membranes of silicon, bilayer nested saddles of epoxy, trilayer epoxy microstructure that resembles a tree. (d) SEM images of 3D multilayer mesostructures with mechanical assist features (left three frames). From left to right: 3D filamentary structure of polyimide, 3D Kirigami box of copper/polyimide bilayers, 3D Origami chair made of epoxy. SEM image of a 3D multilayer mesostructure with entanglements made of copper/polyimide bilayers (the fourth frame from the left). The optical image of a 3D mesostructure with coherently coupled multilayers via selective bonding of copper/polyethylene terephthalate bilayers (the outmost right panel). The scale bars of SEM and optical images are 600  $\mu\text{m}$  and 5 mm, respectively. (For interpretation of the references to color in this figure legend, the reader is referred to the web version of this article.)  
Source: Reproduced from Yan et al. [32], with permission from American Association for the Advancement of Science.

three panels in Fig. 3(c) are 2D precursors. The bottom ones are SEM images of related 3D Origami structures of inverse pyramids (gold/epoxy bilayers, left frame), windmills (silicon/epoxy bilayers, middle frame) and semi-ellipsoids (silicon/epoxy bilayers, right frame). Multiple, hierarchical forms of folding are also possible with appropriate choices in design. The left frames in Fig. 3(d) demonstrate a classical Miura–Origami structure. Combining these ideas with the Kirigami design principles described in the previous section further expands the diversity of realizable mesostructures. As an example, a hexagonal array of hexagonal prisms can be formed by introducing Kirigami lattice cuts (Fig. 3(d), right frame).

#### 2.4. Assembly of 3D overlapping, nested and entangled networks

The assembly of 3D filamentary, Kirigami and Origami mesostructures rely on the compressive buckling of single-layer 2D precursors. The most recent advance is in the development of a

set of fabrication techniques and design concepts for utilizing releasable, multilayer 2D precursors to access classes of 3D geometries that are qualitatively more complex than those of previous reports [29–31]. Examples include dense architectures with nested layouts, controlled points of entanglement, and other previously unobtainable layouts [32].

In this approach, layer-by-layer transfer printing techniques allow assembly of releasable, 2D precursors with different shapes, dimensions and materials into multilayer constructs with high alignment precision. Selective bonding of each of these layers to one another, and to an underlying prestrained assembly substrate enables the formation of 3D multilayer mesostructures by compressive buckling. An example that consists of 3D trilayer nested cages of silicon and epoxy hybrids appear in Fig. 4(a) and (b). Here, each layer independently undergoes a 2D to 3D transformation. The corresponding experimental result appears in the outmost left panel of Fig. 4(c), in which the middle layer (gray) is silicon and the bottom and upper layers (yellow)

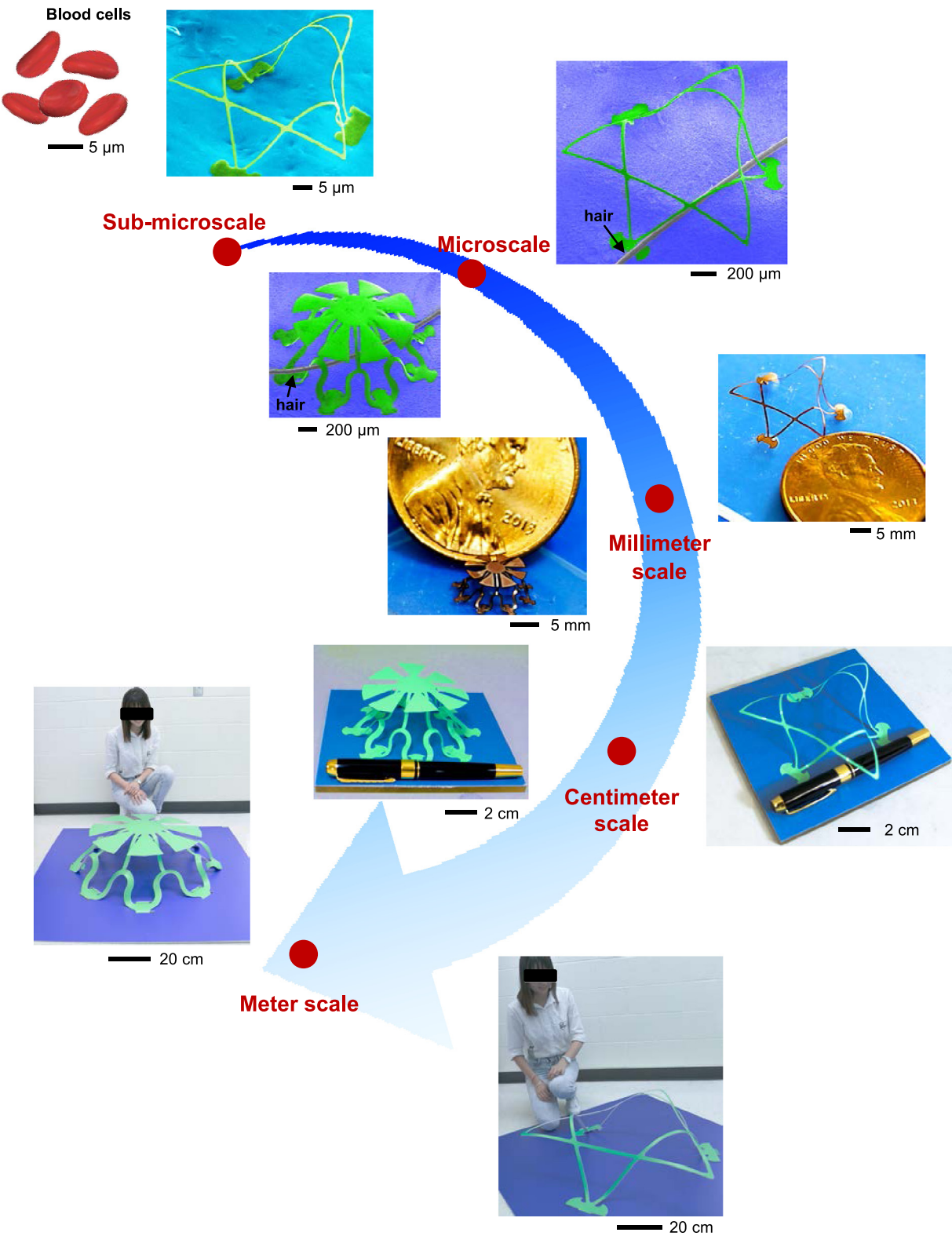


**Fig. 5.** 3D starfish-like and jellyfish-like mesostructures spanning a wide range of length scales.

are epoxy. Fig. 4(c) (right four panels) provides an additional four examples of 3D multilayer mesostructures with separated configurations, including, from left to right, nested boxes of silicon, nested membranes of silicon, bilayer saddles of epoxy, and trilayer trees of epoxy. 3D multilayer mesostructures that incorporate features designed specifically for mechanical interactions between layers are also possible. Fig. 4(d) (left three panels) shows 3D

mesostructures with interacting bilayers in polyimide (green color), epoxy (yellow color), and copper/ polyimide bilayers (orange color). Here, interactions with the overlying layers mechanically assist the assembly process, and provide structural support to the final 3D configuration. In a further level of sophistication, interwoven multilayers can serve as 2D precursors (the fourth panel in Fig. 4(d), copper/polyimide bilayers), to

yield entangled 3D frameworks. An additional design option involves multilayers coherently coupled to one another at selected bonding sites, as shown in the outmost right panel in Fig. 4(d), copper/polyethylene terephthalate bilayers, to yield expanded versatility.

### 2.5. Assembly of 3D structures in variety of materials spanning wide length scales

A key appealing aspect of these general concepts in 3D assembly is that they can be implemented across a broad range of length scales with nearly any type of material, simply through selection of suitable techniques to form the 2D precursors. Fig. 5 highlights two types of 3D structures, a starfish- and a jellyfish-like structure, formed in different materials over an exceptionally broad range of length scales ( $\varepsilon_{pre} \approx 50\%$  for all cases here). In particular, the five 3D starfish-like structures shown here have characteristic dimensions ranging from submicron, micron, millimeter, centimeter to meter scales. The smallest case consists of silicon nanoribbons with thicknesses of 100 nm and widths of 800 nm, at a scale that is similar to that of human red blood cells. Here, deep-ultraviolet photolithography and reactive ion etching formed the 2D precursor. A corresponding microscale version of this same structure results from the use of a 2D precursor formed directly by photolithographically patterning a film of polyimide (10  $\mu\text{m}$  in thickness), where the size scale is comparable to that of a human hair. Mechanical/laser cutting techniques can yield 2D precursors with millimeter-, centimeter- and meter-scale dimensions, with examples in copper (9  $\mu\text{m}$  in thickness) and polyimide (12  $\mu\text{m}$  in thickness) bilayers, polyester films (100  $\mu\text{m}$  in thickness), and polyvinyl chloride boards (3 mm in thickness). By utilizing similar fabrication techniques, 3D jellyfish-like structures with dimensions over the same broad range are also possible, as illustrated in Fig. 5. The capability of assembling 3D structures in variety of advanced materials across wide length scales suggest potential across a diverse collection of applications.

## 3. Conclusion and outlook

This review summarizes recent progress in the deterministic assembly of complex, 3D mesostructures in advanced materials via compressive buckling. As is evident from the examples presented in this article, an exceptionally large number of 3D structures can be achieved using this approach. Key mechanics design concepts and fabrication techniques underpin access to 3D filamentary, Kirigami, Origami and multilayer mesostructures. These advances provide a general but powerful foundation for scientists and engineers in different research areas to explore 3D design options with high-levels of complexity and targeted geometries using broad sets of functional materials, including device-grade silicon, metals, polymers and their hybrids, spanning wide length scales from sub-micron to meter dimensions. Future opportunities lie in broadening the material versatility to other high-quality semiconductors, piezoelectric materials, natural biomaterials, living cells, and 2D layered materials, reducing the lateral dimensions of 3D structures to nanoscale, and increasing the structural diversity and complexity by combining with other techniques of making 3D structures such as 3D printing and self-assembly. In addition to previously reported 3D electronic and optical devices (i.e., inductors [29], optical shutters [30], and near field communication devices [32]) that are mechanically tunable, future application possibilities are in active scaffolds for cells/tissues engineering, thermal and mechanical energy harvesters, micro/nanoscale robotics, stretchable electronics, transient 3D electronic and optic devices, 3D antenna for optogenetics, biochemical sensors, and many others.

## Acknowledgments

We acknowledge the financial support from the Air Force Office of Scientific Research (AFOSR) MURI FA9550-08-1-0407.

## References

- [1] R.R. Syms, E.M. Yeatman, V.M. Bright, G.M. Whitesides, Surface tension-powered self-assembly of microstructures—the state-of-the-art, *J. Microelectromech. Syst.* 12 (2003) 387–417.
- [2] R.J. Wood, The challenge of manufacturing between macro and micro, *Am. Sci.* 102 (2014) 124.
- [3] J. Rogers, Y. Huang, O.G. Schmidt, D.H. Gracias, Origami MEMS and NEMS, *MRS Bull.* 41 (2016) 123–129.
- [4] T.G. Leong, C.L. Randall, B.R. Benson, N. Bassik, G.M. Stern, D.H. Gracias, Tetherless thermobiochemically actuated microgrippers, *Proc. Natl. Acad. Sci.* 106 (2009) 703–708.
- [5] R. Feiner, L. Engel, S. Fleischer, M. Malki, I. Gal, A. Shapira, Y. Shacham-Diamand, T. Dvir, Engineered hybrid cardiac patches with multifunctional electronics for online monitoring and regulation of tissue function, *Nature Mater.* 15 (2016) 679–685.
- [6] X. Dai, W. Zhou, T. Gao, J. Liu, C.M. Lieber, Three-dimensional mapping and regulation of action potential propagation in nanoelectronics-innervated tissues, *Nature Nanotechnol.* 11 (2016) 776–782.
- [7] L. Xu, S.R. Gutbrod, A.P. Bonifas, Y. Su, M.S. Sulkin, N. Lu, H.J. Chung, K.I. Jang, Z. Liu, M. Ying, C. Liu, R.C. Webb, J.S. Kim, J.I. Laughner, H. Cheng, Y. Liu, A. Ameen, J.W. Jeong, G.T. Kim, Y. Huang, I.R. Efimov, J.A. Rogers, 3D multifunctional integumentary membranes for spatiotemporal cardiac measurements and stimulation across the entire epicardium, *Nature Commun.* 5 (2014) 3329.
- [8] P.V. Braun, Materials chemistry in 3D templates for functional photonics, *Chem. Mater.* 26 (2013) 277–286.
- [9] Z. Fan, H. Razavi, J.W. Do, A. Moriwaki, O. Ergen, Y.L. Chueh, P.W. Leu, J.C. Ho, T. Takahashi, L.A. Reichert, S. Neale, K. Yu, M. Wu, J.W. Ager, A. Javey, Three-dimensional nanopillar-array photovoltaics on low-cost and flexible substrates, *Nature Mater.* 8 (2009) 648–653.
- [10] T.S. Arthur, D.J. Bates, N. Cirigliano, D.C. Johnson, P. Malati, J.M. Mosby, E. Perre, M.T. Rawls, A.L. Prieto, B. Dunn, Three-dimensional electrodes and battery architectures, *MRS Bull.* 36 (2011) 523–531.
- [11] H. Ning, J.H. Pikel, R. Zhang, X. Li, S. Xu, J. Wang, J.A. Rogers, W.P. King, P.V. Braun, Holographic patterning of high-performance on-chip 3D lithium-ion microbatteries, *Proc. Natl. Acad. Sci.* 112 (2015) 6573–6578.
- [12] H. Jiang, P.S. Lee, C. Li, 3D carbon based nanostructures for advanced supercapacitors, *Energy Environ. Sci.* 6 (2013) 41–53.
- [13] J. Valentine, S. Zhang, T. Zentgraf, E. Ulin-Avila, D.A. Genov, G. Bartal, X. Zhang, Three-dimensional optical metamaterial with a negative refractive index, *Nature* 455 (2008) 376–379.
- [14] J.K. Gansel, M. Thiel, M.S. Rill, M. Decker, K. Bade, V. Saile, G.v. Freymann, S. Linden, M. Wegener, Gold helix photonic metamaterial as broadband circular polarizer, *Science* 325 (2009) 1513–1515.
- [15] D. Chanda, K. Shigeta, S. Gupta, T. Cain, A. Carlson, A. Mihi, A.J. Baca, G.R. Bogart, P. Braun, J.A. Rogers, Large-area flexible 3D optical negative index metamaterial formed by nanotransfer printing, *Nature Nanotechnol.* 6 (2011) 402–407.
- [16] J.C. Nawroth, H. Lee, A.W. Feinberg, C.M. Ripplinger, M.L. McCain, A. Grosberg, J.O. Dabiri, K.K. Parker, A tissue-engineered jellyfish with biomimetic propulsion, *Nature Biotechnol.* 30 (2012) 792–797.
- [17] N.W. Bartlett, M.T. Tolley, J.T. Overvelde, J.C. Weaver, B. Mosadegh, K. Bertoldi, G.M. Whitesides, R.J. Wood, A 3D-printed, functionally graded soft robot powered by combustion, *Science* 349 (2015) 161–165.
- [18] S.J. Park, M. Gazzola, K.S. Park, S. Park, V. Di Santo, E.L. Blevins, J.U. Lind, P.H. Campbell, S. Dauth, A.K. Capulli, F.S. Pasqualini, S. Ahn, A. Cho, H. Yuan, B.M. Maoz, R. Vijaykumar, J.W. Choi, K. Deisseroth, G.V. Lauder, L. Mahadevan, K.K. Parker, Phototactic guidance of a tissue-engineered soft-robotic ray, *Science* 353 (2016) 158–162.
- [19] S.V. Murphy, A. Atala, 3D bioprinting of tissues and organs, *Nature Biotechnol.* 32 (2014) 773–785.
- [20] M.A. Skylar-Scott, S. Gunasekaran, J.A. Lewis, Laser-assisted direct ink writing of planar and 3D metal architectures, *Proc. Natl. Acad. Sci.* 113 (2016) 6137–6142.
- [21] B.H. Cumpston, S.P. Ananthavel, S. Barlow, D.L. Dyer, J.E. Ehrlich, L.L. Erskine, A.A. Heikal, S.M. Kuebler, I.Y.S. Lee, D. McCord-Maughon, J. Qin, H. Röckel, M. Rumi, X.L. Wu, S.R. Marder, J.W. Perry, Two-photon polymerization initiators for three-dimensional optical data storage and microfabrication, *Nature* 398 (1999) 51–54.
- [22] M. Farsari, B.N. Chichkov, Materials processing: Two-photon fabrication, *Nat. Photonics* 3 (2009) 450–452.
- [23] A. Kuzyk, R. Schreiber, Z. Fan, G. Pardatscher, E.M. Roller, A. Högele, F.C. Simmel, A.O. Govorov, T. Liedl, DNA-based self-assembly of chiral plasmonic nanostructures with tailored optical response, *Nature* 483 (2012) 311–314.
- [24] J.V. Timonen, M. Latikka, L. Leibler, R.H. Ras, O. Ikkala, Switchable static and dynamic self-assembly of magnetic droplets on superhydrophobic surfaces, *Science* 341 (6143) (2013) 253–257.
- [25] J. Yang, D. Yan, T.S. Jones, Molecular template growth and its applications in organic electronics and optoelectronics, *Chem. Rev.* 115 (2015) 5570–5603.

- [26] W. Gao, X. Feng, A. Pei, C.R. Kane, R. Tam, C. Hennessy, J. Wang, Bioinspired helical microswimmers based on vascular plants, *Nano Lett.* 14 (2013) 305–310.
- [27] O.G. Schmidt, K. Eberl, Nanotechnology: Thin solid films roll up into nanotubes, *Nature* 410 (2001) 168.
- [28] X. Zhang, C.L. Pint, M.H. Lee, B.E. Schubert, A. Jamshidi, K. Takei, H. Ko, A. Gillies, R. Bardhan, J.J. Urban, M. Wu, R. Fearing, A. Javey, Optically- and thermally-responsive programmable materials based on carbon nanotube-hydrogel polymer composites, *Nano Lett.* 11 (2011) 3239–3244.
- [29] S. Xu, Z. Yan, K.I. Jang, W. Huang, H. Fu, J. Kim, Z. Wei, M. Flavin, J. McCracken, R. Wang, A. Badea, Y. Liu, D. Xiao, G. Zhou, J. Lee, H.U. Chung, H. Cheng, W. Ren, A. Banks, X. Li, U. Paik, R.G. Nuzzo, Y. Huang, Y. Zhang, J.A. Rogers, Assembly of micro/nanomaterials into complex, three-dimensional architectures by compressive buckling, *Science* 347 (2015) 154–159.
- [30] Y. Zhang, Z. Yan, K. Nan, D. Xiao, Y. Liu, H. Luan, H. Fu, X. Wang, Q. Yang, J. Wang, W. Ren, H. Si, F. Liu, L. Yang, H. Li, J. Wang, X. Guo, H. Luo, L. Wang, Y. Huang, J.A. Rogers, A mechanically driven form of Kirigami as a route to 3D mesostructures in micro/nanomembranes, *Proc. Natl. Acad. Sci.* 112 (2015) 11757–11764.
- [31] Z. Yan, F. Zhang, J. Wang, F. Liu, X. Guo, K. Nan, Q. Lin, M. Gao, D. Xiao, Y. Shi, Y. Qiu, H. Luan, J.H. Kim, Y. Wang, H. Luo, M. Han, Y. Huang, Y. Zhang, J.A. Rogers, Controlled mechanical buckling for origami-inspired construction of 3D microstructures in advanced materials, *Adv. Funct. Mater.* 26 (2016) 2629–2639.
- [32] Z. Yan, F. Zhang, F. Liu, M. Han, D. Ou, Y. Liu, Q. Lin, X. Guo, H. Fu, Z. Xie, M. Gao, Y. Huang, J.H. Kim, Y. Qiu, K. Nan, J. Kim, P. Gutruf, H. Luo, A. Zhao, K.C. Hwang, Y. Huang, Y. Zhang, J.A. Rogers, Mechanical assembly of complex, 3D mesostructures from releasable multilayers of advanced materials, *Sci. Adv.* 2 (2016) e1601014.
- [33] M.A. Meitl, Z.T. Zhu, V. Kumar, K.J. Lee, X. Feng, Y.Y. Huang, I. Adesida, R.G. Nuzzo, J.A. Rogers, Transfer printing by kinetic control of adhesion to an elastomeric stamp, *Nature Mater.* 5 (2006) 33–38.
- [34] S. Kim, J. Wu, A. Carlson, S.H. Jin, A. Kovalsky, P. Glass, Z. Liu, N. Ahmed, S.L. Elgan, W. Chen, P.M. Ferreira, M. Sitti, Y. Huang, J.A. Rogers, Microstructured elastomeric surfaces with reversible adhesion and examples of their use in deterministic assembly by transfer printing, *Proc. Natl. Acad. Sci.* 107 (2010) 17095–17100.